Amide - Based Ionic Liquid Electrolytes for Alkali - Metal - Ion Rechargeable Batteries

AUTHOR(S):

Yamamoto, Takayuki; Nohira, Toshiyuki

CITATION:

Yamamoto, Takayuki ...[et al]. Amide - Based Ionic Liquid Electrolytes for Alkali - Metal - Ion Rechargeable Batteries. The Chemical Record 2023, 23(8): e202300169.

ISSUE DATE:

2023-08

URL:

http://hdl.handle.net/2433/284729

Personal Account

THE CHEMICAL RECORD

doi.org/10.1002/tcr.202300169
tcr.wiley-vch.de

Amide-Based Ionic Liquid Electrolytes for Alkali-Metal-Ion Rechargeable Batteries

Takayuki Yamamoto and Toshiyuki Nohira*[a]

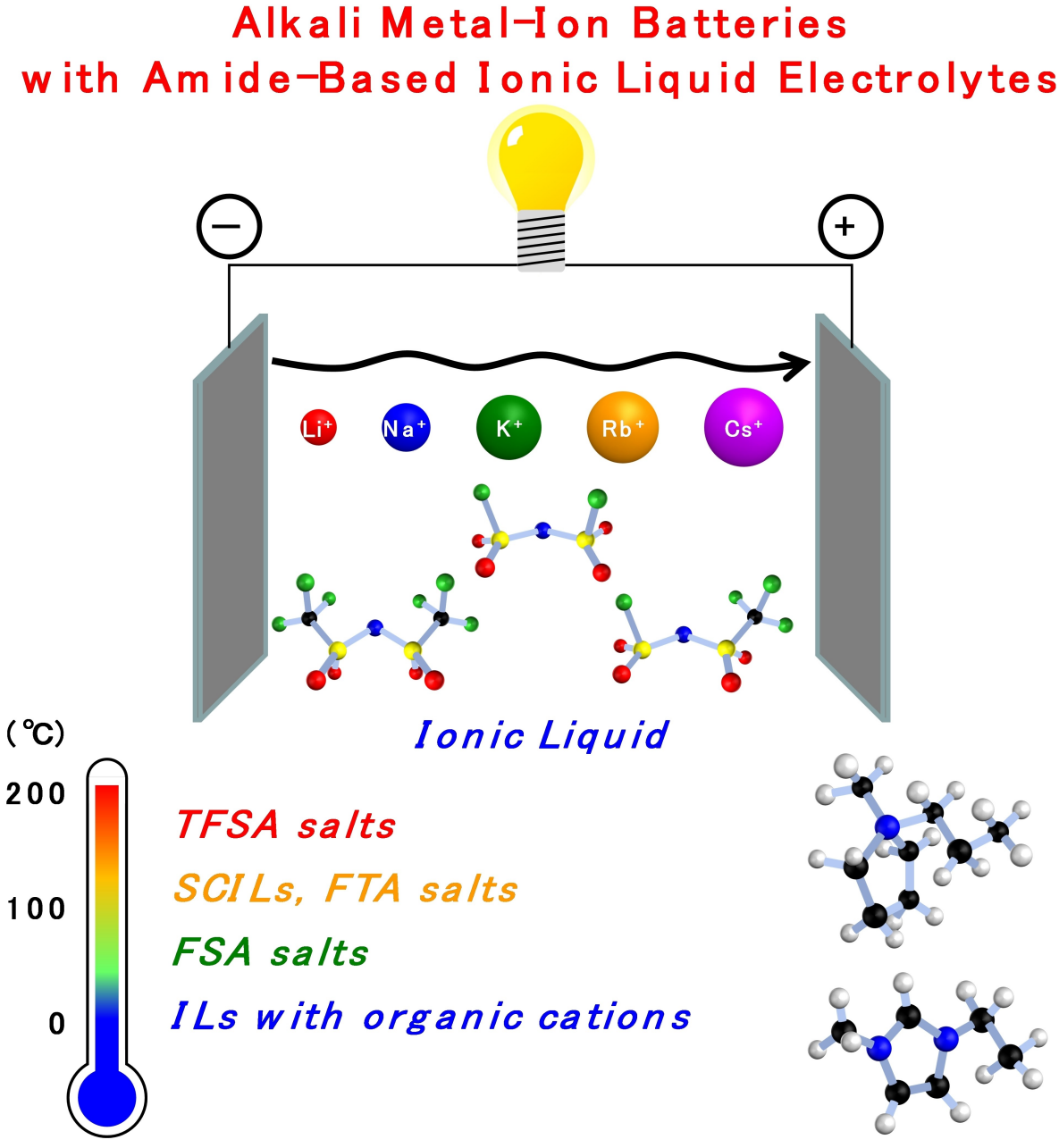

Abstract: Ionic liquids (ILs) have a wide variety of applications in energy storage and material production. ILs are composed of only cations and anions, without any molecular solvents, and are generally known as "designer liquids (solvents)" because their physicochemical properties can be tuned by the combination of ionic species. In recent several decades, research and development activities of rechargeable batteries have garnered considerable attention because certain groups of ILs exhibit high electrochemical stability and moderate ionic conductivity, rendering them suitable for application in high-voltage batteries. ILs with amide anions are representative electrolytes and are extensively researched by many research groups, including our group. This paper focuses on amide-based ILs as electrolytes for alkali-metal-ion rechargeable batteries, introducing their history, characteristics, and existing challenges to be addressed.

Keywords: Ionic liquid, Electrolyte, Alkali-metal-ion battery, Lithium-ion battery, Sodium-ion battery

1. Introduction

With the development of lithium-ion batteries, which are used in portable electronic devices, rechargeable batteries have emerged as a critical component in our society, and the demand for their large-scale application, such as in electric vehicles and stationary batteries, is increasing. However, the flammable and volatile characteristics of the organic solvents used for electrolytes increase the risk of ignition accidents, and the uneven distribution of cobalt and lithium resources intrinsically limits the mass production of large-scale batteries because these rare metals are required for constructing positive electrodes. These circumstances have led many researchers to a paradigm shift from conventional organic-solvent-based electrolytes to ionic liquids (ILs) or molten salts, and from lithium ions to sodium and potassium ions as charge carriers.[1]

ILs are employed as universal reaction media because of their unique chemical and thermal stability, negligible volatility, and ionic conductivity. Their potential applications extend to electrochemical energy storage devices (batteries, fuel cells, and capacitors),[2] material production,[3] carbon capture and storage,[4] biorefinery,[5] and biochemistry.[6] Historically, ILs have been referred to as room-temperature (or low-temperature) molten salts to distinguish them from high-temperature molten salts, which are mostly composed of inorganic ion species. Although their boundaries remain unclear, molten salts with melting points below 373 K are generally termed "ionic liquids".[2a] In general, melting points decrease when small and hard ions (e.g., halide ions) are replaced with bulky and soft ions (e.g., organic ions). Applying rigid definitions to ILs is difficult because the IL research field is expanding as new types of IL derivatives, such as solvated ILs, which contain neutral solvents, are emerging.[2a,7] However, most ILs and their derivatives exhibit high ionicity and low volatility under typical conditions. Therefore, they are suitable electrolytes for next-generation rechargeable batteries and provide excellent safety.

The research and development on rechargeable batteries using molten salts and ILs began from studies on the behaviors of metal chloride and bromide molten salts,[8] which are known as "molten salt batteries" or "thermal batteries" operating above 500 K. Since the 1990s, room-temperature molten salts (ILs) containing imidazolium cations and chloroaluminate anions have been reported as candidate electrolytes for novel lithium batteries operating at room temperature.[9] Simultaneously, the physicochemical and electrochemical properties were reported for imidazolium ILs with various anion species, such as BF_4^-, PF_6^-, AsF_6^-, $C(SO_2CF_3)_3^-$, $SO_3CF_3^-$ (triflate, TfO^-, derived from trifluoromethanesulfonate (TfO)), and $N(SO_2CF_3)_2^-$ ($TFSA^-$, derived from bis(trifluoromethylsulfonyl)amide (TFSA)).[10] Among them, ILs composed of amide anions (such as $TFSA^-$) exhibit superior ionic conductivity and electrochemical stability and are therefore the mainstream battery electrolytes.

Apart from utilizing organic cations, such as the imidazolium series, a strategy to realize batteries operating at low temperatures is to combine several metal salts. For example, the melting points of Li[TFSA] and K[TFSA] are 506 and 472 K, respectively, and their mixture at the eutectic composition of x(Li[TFSA]) = 0.43 (x: molar ratio) melts at 423 K.[11a] A ternary mixture of Li[TFSA], K[TFSA], and Cs[TFSA] in a molar ratio of 20 : 10 : 70 melts at 419 K, and a Li/$LiFePO_4$ cell works efficiently with this melt at 423 K.[11b] Furthermore, a Na[TFSA]–Cs[TFSA] mixture at x(Na[TFSA]) = 0.10 melts at 390 K and can function as an electrolyte for sodium batteries, as demonstrated by the

[a] *T. Yamamoto, T. Nohira*
Institute of Advanced Energy, Kyoto University,
Gokasho, Uji, Kyoto 611-0011, Japan
E-mail: nohira.toshiyuki.8r@kyoto-u.ac.jp

performance of a $Na/NaCrO_2$ cell at 423 K.[11c] However, the melting points of M[TFSA] mixtures (M = alkali metal) remain above 373 K. Several years after the development of TFSA-based ILs, a new class of electrolyte with a simple amide anion, $N(SO_2F)_2^-$ (FSA^-, derived from bis(fluorosulfonyl)amide (FSA)), has attracted substantial attention owing to its low melting points.[12] The potential of other anions with asymmetric structures, such as $N(SO_2F)(SO_2CF_3)^-$ (FTA^-, derived from (fluorosulfonyl)(trifluoromethylsulfonyl)amide (FTA)), have also been explored to decrease the melting points of ILs.[13] The structures of representative ions in ILs are summarized in Figure 1. This comprehensive paper introduces representative research on alkali-metal-ion batteries utilizing amide-based ILs, including the contributions of the authors, and discusses the feasibility for their practical applications and potential issues.

2. TFSA-Based ILs

TFSA-based ILs are a widely used class of battery electrolytes because they are easy to handle and have a high electrochemical stability and moderate ionic conductivity. Although imidazolium-based compounds have been well studied, they have insufficient reductive stability owing to their aromatic ring, which potentially hinders their application in the construction of high-voltage batteries. Since 2000, the application of quaternary ammonium ILs as battery electrolytes has attracted attention, and their physicochemical properties have been investigated to overcome the aforementioned issues.[14]

2.1. Lithium-Ion Batteries

In 2003, Sakaebe and Matsumoto reported the charge–discharge performance of $Li/LiCoO_2$ cells that used Li[TFSA]–[C_3C_1pip][TFSA] (C_3C_1pip = *N*-methyl-*N*-propylpiperidinium) as the electrolyte (Figure 2). Their results demonstrated that the IL was a promising electrolyte for lithium batteries.[15a] Garcia et al. demonstrated the performance of a $Li_4Ti_5O_{12}/LiCoO_2$ cell that used Li[TFSA]–[C_2C_1im][TFSA] (C_2C_1im = 1-ethyl-3-methylimidazolium) as the electrolyte in a temperature range of 278–353 K.[15b] At 298 K, the rate capability of the cell was higher than that achieved with Li[BF_4]–[C_2C_1im][BF_4] but less than that obtained with Li[TFSA] in ethylene carbonate/dimethyl carbonate, which is a typical organic solvent-based electrolyte. In another study, Sakaebe et al. elucidated the effects of cationic structures on the properties of $Li/LiCoO_2$ cells and concluded that the stability against Li metal determined the charge–discharge performance.[15c] According to the thermal stability tests of various electrolytes in contact with Li metal and $Li_{1-x}CoO_2$, which were performed by imitating the conditions of practical batteries, Li[TFSA]–[C_3C_1pip][TFSA] IL showed higher thermal stability than organic solvent-based electrolytes.[15d] To enhance the performance of lithium metal negative electrodes, Howlett et al. used X-ray photoelectron spectroscopy, Fourier-transform infrared spectroscopy, Raman spectroscopy, and electrochemical impedance spectroscopy to examine the nature of the solid electrolyte interphase (SEI) formed on the lithium metal surface in the Li[TFSA]–[C_3C_1pyrr][TFSA] electrolyte (C_3C_1pyrr = *N*-methyl-*N*-propylpyrrolidinium).[15e] They pro-

Takayuki Yamamoto is an Assistant Professor at Kyoto University. He graduated from Graduate School of Energy Science, Kyoto University, and received his Ph.D. degree in 2016. He worked as JSPS Research Fellowship for Young Scientist (2015–2016), and Researcher in the office of Society Academia Collaboration for Innovation, Kyoto University (2016–2017). He moved to Institute of Advanced Energy, Kyoto University as Assistant Professor in 2017. He was awarded Young Researcher Award of The Electrochemical Society of Japan (Sano Award) in 2022. His current research focuses on rechargeable batteries using ionic liquids and various charge carriers.

Toshiyuki Nohira is a Professor at Kyoto University. He received his Ph.D. from Kyoto University in 1998. He worked as Assistant Professor (1998–) and Associate Professor (2007–) at Graduate School of Energy Science, Kyoto University. He was promoted to Professor of Institute of Advanced Energy, Kyoto University in 2015. He was awarded the Young Scientists' Prize of the Commendation for Science and Technology by the Minister of Education, Culture, Sports, Science and Technology of Japan (2009), and Scientific Achievement Award of The Electrochemical Society of Japan (2020). His research interests are electrochemical applications of molten salts and ionic liquids in the fields of materials science and energy science.

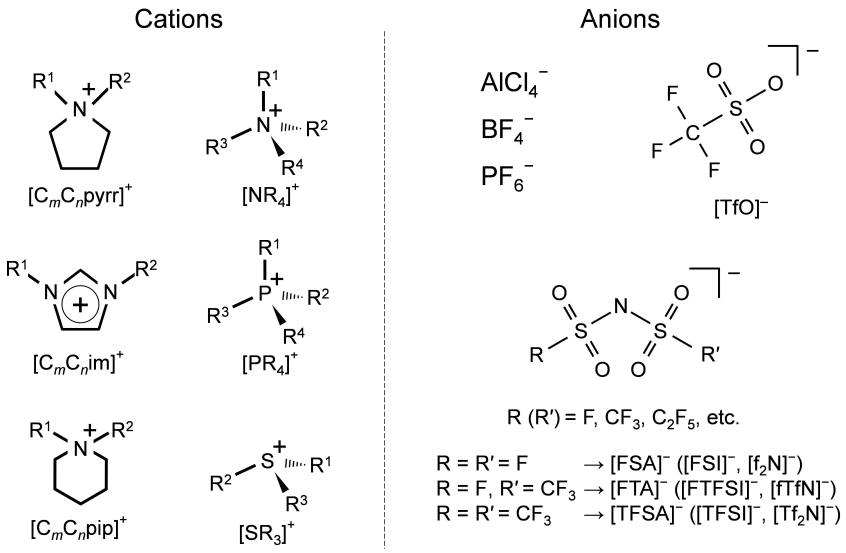

Figure 1. Representative cations and anions contained in ILs and their structures.

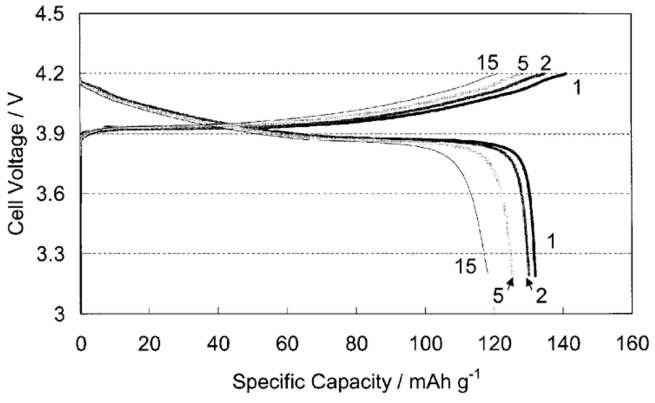

Figure 2. Charge-discharge curves of a Li/Li[TFSA]–[C$_3$C$_1$pip][TFSA]/LiCoO$_2$ cell. Reproduced from Ref. [15a] with permission from Elsevier.

posed a model for the SEI layer formed on electrochemically deposited lithium, which was different from the native species present on the surface of commercially available lithium metal. A major drawback of the TFSA-based ILs is their poor compatibility with graphite negative electrodes,[15f] which are currently used in most practical lithium-ion batteries. Therefore, a majority of studies on lithium-ion batteries have gradually shifted their focus to FSA-dominant ILs.

2.2. Sodium-Ion and Potassium-Ion Batteries

In the mid-2000s, following the pioneering work conducted in the 1980 s,[16] sodium secondary batteries attracted significant attention owing to the increasing demand for lithium-ion batteries.[17] Sodium resources are abundant in the Earth's crust and seawater; hence, its depletion is not a concern, in contrast to the case of lithium and cobalt.[18] Monti et al. reported the physicochemical properties of Na[TFSA]–[C$_2$C$_1$im][TFSA] and Na[TFSA]–[C$_4$C$_1$im][TFSA] (C$_4$C$_1$im = 1-butyl-3-methylimidazolium) ILs.[19] At the same time, several studies were conducted on Na[TFSA]–[C$_4$C$_1$pyrr][TFSA] (C$_4$C$_1$pyrr = *N*-butyl-*N*-methylpyrrolidinium).[20] Wongittharom et al. demonstrated the charge–discharge performance of Na/NaFePO$_4$ cells.[20b] It is well known that sodium cannot be reversibly intercalated into graphite;[21] hence, hard carbon (HC) is used as the negative electrode for sodium-ion batteries with organic solvent-based electrolytes.[22] A few studies have been conducted on the performance of HC negative-electrodes with pure TFSA ILs; however, the presence of TFSA$^-$ anions adversely affects the HC performance.[23]

Recently, the possibility of potassium-ion batteries has been explored considering the abundance of potassium resources in the Earth's crust and their potentially high operating voltages.[24] Based on our previous report on Li[TFSA]–K[TFSA]–Cs[TFSA] system,[11b] the cathodic limit of the melt at 423 K is the lithium metal deposition/dissolution reaction, which indicates that the redox potential of K$^+$/K is more negative than that of Li$^+$/Li. Thus, by employing IL electrolytes, the construction of potassium-ion batteries with operating voltages similar to or higher than those of lithium-ion batteries is possible. Masese and Yoshii et al. reported the properties of K[TFSA]–[C$_3$C$_1$pyrr][TFSA] IL and the charge–discharge performance of several positive electrodes, such as $K_{2/3}Ni_{2/3}Te_{1/3}O_2$ (Figure 3) and $K_{0.4}Fe_{0.5}Mn_{0.5}O_2$ electrodes.[25]

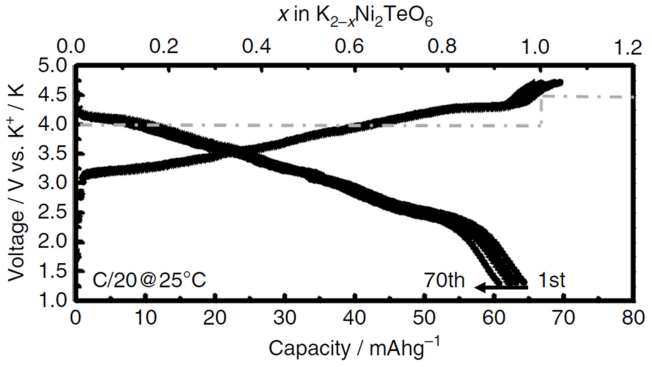

Figure 3. Charge–discharge curves of a $K/K_2Ni_2TeO_6$ half-cell using an IL electrolyte (0.5 M K[TFSA] in [C_3C_1pyrr][TFSA]). Reproduced from Ref. [25a] with permission from Nature Portfolio.

3. FSA-Based ILs

ILs composed of FSA^- anion appeared as a new class of electrolytes owing to their high ionic conductivities and low melting points (Table 1), which are derived from high dissociation abilities. Moreover, FSA-based ILs are known to realize lower interfacial resistance at the electrode/electrolyte interface, which was explained by the SEI film formation with good compatibility.[23,26] Therefore, FSA-based ILs are among the commonly used electrolytes in battery studies thus far.

3.1. Lithium-Ion Batteries

In 2006, Matsumoto et al. compared the physicochemical properties of Li[TFSA]–[Ocat][X] (Ocat = C_2C_1im, C_3C_1pyrr, and C_3C_1pip; X = TFSA and FSA) with Li[TFSA] concentration of 0.3 mol kg^{-1} and the performance of $Li/LiCoO_2$ batteries (Figure 4).[27a] Compared to pure TFSA ILs, those containing FSA^- anion showed higher ionic conductivities and lower viscosities. Moreover, the $Li/LiCoO_2$ cells with ILs containing FSA^- ions exhibited superior capability, which reflects their electrolytic properties. Ishikawa et al. reported that graphite negative electrodes could function with electrolytes of 0.8 M Li[TFSA] in [C_2C_1im][FSA] or [C_3C_1pyrr][FSA] ILs.[15f] In contrast, pure TFSA IL, 0.8 M Li[TFSA]–[C_2C_1im][TFSA], gives the poor reversibility of Li^+ intercalation/deintercalation into/from graphite (Figure 5).[15f] Although the performance appeared to improve after replacing $C_2C_1im^+$ with $C_3C_1pyrr^+$ in the IL electrolytes,[26a] $TFSA^-$ anions destabilized the performance of the graphite negative electrodes. Ishikawa et al. explained the phenomenon was attributed to the difference between the electrolyte/electrolyte interfacial liquid structures in Li[TFSA]–[C_2C_1im][TFSA] and Li[TFSA]–[C_2C_1im][FSA] ILs.[27b] In 2008, Guerfi et al. reported the performance of Li/graphite and $Li/LiFePO_4$ half-cells using pure FSA ILs, Li[FSA]–[Ocat][FSA] (Ocat = C_2C_1im, C_3C_1pyrr), where the reversible capacities were comparable to those of organic solvent-based electrolytes.[28] However, the rate performance of these IL-based batteries was inferior to that of organic solvent-based electrolytes, which remains an issue to be solved. A possible application of IL batteries is in space engineering, which requires cells with high thermal and radiation stabilities and negligible risks of vaporization and ignition accidents. Prototype graphite/$LiNi_{1/3}Mn_{1/3}Co_{1/3}O_2$ cells with Li[FSA]–[C_3C_1pyrr][FSA] electrolyte was successfully operated in a demonstration module on a micro-satellite launched in 2014.[29] Based on structural studies conducted on Li[X]–[C_2C_1im][X] (X = TFSA and FSA),[30] the stable complex ions in the FSA-based IL are $[Li(FSA)_2]^-$ and $[Li(FSA)_3]^{2-}$, and the dominant species easily fluctuates with temperature, owing to the presence of monodentate ligands. In contrast, $[Li(TFSA)_2]^-$ is rather stable in TFSA-based ILs, in which Li^+ is coordinated only by bidentate ligands. These structural differences may decrease the melting points and increase the solubility of Li salts at room temperature in FSA-based ILs.[31]

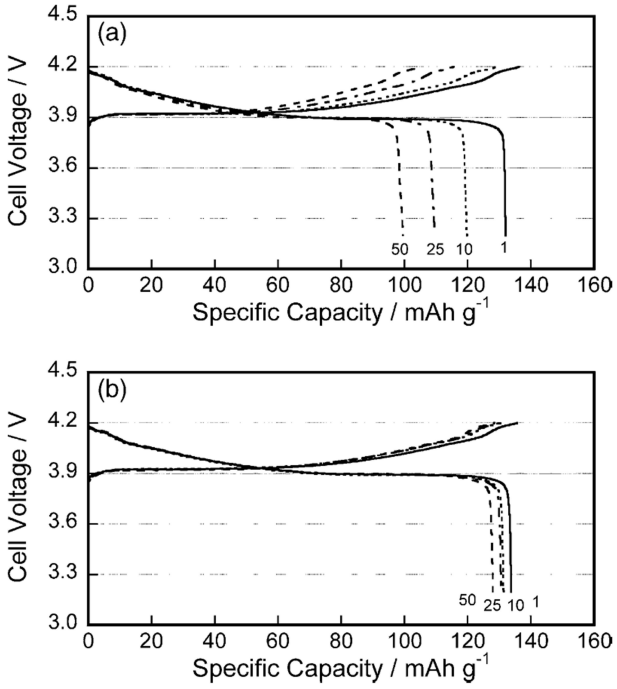

Figure 4. Charge–discharge curves of $Li/LiCoO_2$ half-cells using 0.3 mol kg^{-1} Li[TFSA]–[Ocat][TFSA] (Ocat = (a) C_2C_1im, (b) C_3C_1pyrr) IL electrolytes. Reproduced from Ref. [27a] with permission from Elsevier.

3.2. Sodium-Ion Batteries

In 2012, we reported the charge–discharge performance of $Na/NaCrO_2$ cells at 353 K with Na[FSA]–K[FSA] (x(Na[FSA]) = 0.56) electrolyte that melts at 334 K (Figure 6).[32]

Table 1. Physicochemical properties of selected ILs at 298 K.*

IL	M salt	M^+ concentration	η/mPa s	σ/mS cm^{-1}	ρ/g cm^{-3}	T_m/K	Ref.
Neat IL							
$[C_2C_1im][TFSA]$	–	–	33	8.3			[27a]
$[C_3C_1pyrr][TFSA]$	–	–	61	3.9			[27a]
$[C_3C_1pip][TFSA]$	–	–	151	1.4			[27a]
$[N_{2225}][TFSA]$	–	–	172	0.98	1.33	<223	[54a]
$[P_{2225}][TFSA]$	–	–	88	1.73	1.32	290	[54a]
$[C_2C_1im][FSA]$	–	–	18	15.4			[27a]
$[C_2C_1im][FSA]$	–	–	19.2	16.4	1.442	263	[39]
$[C_3C_1pyrr][FSA]$	–	–	40	8.2			[27a]
$[C_3C_1pyrr][FSA]$	–	–	40.6	8.4	1.3391	269	[37]
$[C_3C_1pip][FSA]$	–	–	95	3.7			[27a]
$[N_{4411}][FSA]$	–	–	100	2.4	1.230	288	[35f]
$[P_{2224}][FSA]$	–	–	62	4.5	1.26	257	[54b]
$[P_{2225}][FSA]$	–	–	70	3.0	1.24	238	[54b]
$[S_{222}][FSA]$	–	–	20	15.3	1.3890		[54c]
$[S_{122}][FSA]$	–	–	24	15.7	1.4504	218	[54c]
$[C_4C_1pyrr][FTA]$	–	–	51.0	4.4	1.357		[50]
Li system							
$[C_2C_1im][TFSA]$	Li[TFSA]	0.3 mol kg^{-1}	55	5.1			[27a]
$[C_3C_1pyrr][TFSA]$	Li[TFSA]	0.3 mol kg^{-1}	130	2.0			[27a]
$[C_3C_1pip][TFSA]$	Li[TFSA]	0.3 mol kg^{-1}	330	0.7			[27a]
$[C_2C_1im][FSA]$	Li[FSA]	0.3 mol kg^{-1}	24	11.0			[27a]
$[C_2C_1im][FSA]$	Li[FSA]	1.110 mol dm^{-3}	36.3	10.1	1.501	254	[55]
$[C_3C_1pyrr][FSA]$	Li[FSA]	0.3 mol kg^{-1}	51	5.5			[27a]
$[C_3C_1pyrr][FSA]$	Li[FSA]	0.987 mol dm^{-3}	71.0	5.0	1.4022		[56]
$[C_3C_1pip][FSA]$	Li[FSA]	0.3 mol kg^{-1}	124	2.5			[27a]
$[C_4C_1pyrr][FTA]$	Li[FTA]	0.820 mol dm^{-3}	117	2.0	1.416	262	[50]
Na system							
$[C_2C_1im][FSA]$	Na[FSA]	1.110 mol dm^{-3}	43.4	8.5	1.519	251	[35d]
$[C_3C_1pyrr][FSA]$	Na[FSA]	0.983 mol dm^{-3}	95	3.6	1.4127		[35e]
$[N_{4411}][FSA]$	Na[FSA]	1.280 mol dm^{-3}	356	0.69	1.354		[35f]
$[C_4C_1pyrr][FTA]$	Na[FTA]	0.819 mol dm^{-3}	149	1.7	1.427		[50]
K, Rb, and Cs systems							
$[C_2C_1im][TFSA]$	K[TFSA]	0.5 mol dm^{-3}	58	5.7	1.559	~255	[25b]
$[C_3C_1pyrr][TFSA]$	K[TFSA]	0.5 mol dm^{-3}	119	2.1	1.474	~280	[25b]
$[C_2C_1im][FSA]$	K[FSA]	1.100 mol dm^{-3}	39.1	10.1	1.523	256	[39]
$[C_3C_1pyrr][FSA]$	K[FSA]	0.977 mol dm^{-3}	78.2	4.8	1.4198	256	[37]
$[C_4C_1pyrr][FTA]$	K[FTA]	0.814 mol dm^{-3}	128	2.2	1.431		[50]
$[C_4C_1pyrr][FTA]$	Rb[FTA]	0.811 mol dm^{-3}	119	2.3	1.464		[50]
$[C_4C_1pyrr][FTA]$	Cs[FTA]	0.806 mol dm^{-3}	97.4	2.6	1.494		[50]

*η: viscosity, σ: ionic conductivity, ρ: density, T_m: melting point

Unlike TFSA-based ILs, this IL is composed entirely of inorganic ions, realizing an electrolyte with high resistance to reduction.[12] Moreover, the production of FSA-based ILs does not require electrolytic fluorination, which is a process that increases the cost of TFSA salt synthesis. Subsequently, we successfully applied several positive and negative electrode materials to sodium batteries using the Na[FSA]–K[FSA] IL electrolyte.[33] At the same time, room-temperature ILs were studied by several research groups.[34] We demonstrated promising results for sodium-ion batteries with Na[FSA]–[Ocat][FSA] (Ocat = C_3C_1pyrr and C_2C_1im) IL electrolytes used in combination with various positive and negative electrodes.[35] The FSA-based ILs were considerably more stable against Na metal in Na/Na symmetric cells possessing lower interfacial resistances and showed negligible color changes even after contact with Na metal for four weeks.[35g] As shown in Figure 7, 27 Ah-class HC/$NaCrO_2$ full-cells can be successfully operated using the Na[FSA]–[C_3C_1pyrr][FSA] electrolyte (x(Na[FSA]) = 0.20) at 298 and 333 K, which indicates the promising feasibility of large-scale sodium-ion batteries.[35h] Moreover, an enhanced battery performance was reported using ILs with high Na^+ ion concentrations.[36] We confirmed the improved rate capability of Na/$NaCrO_2$ half-cells at 363 K when the molar fraction of Na salt (x(Na[FSA])) in Na-

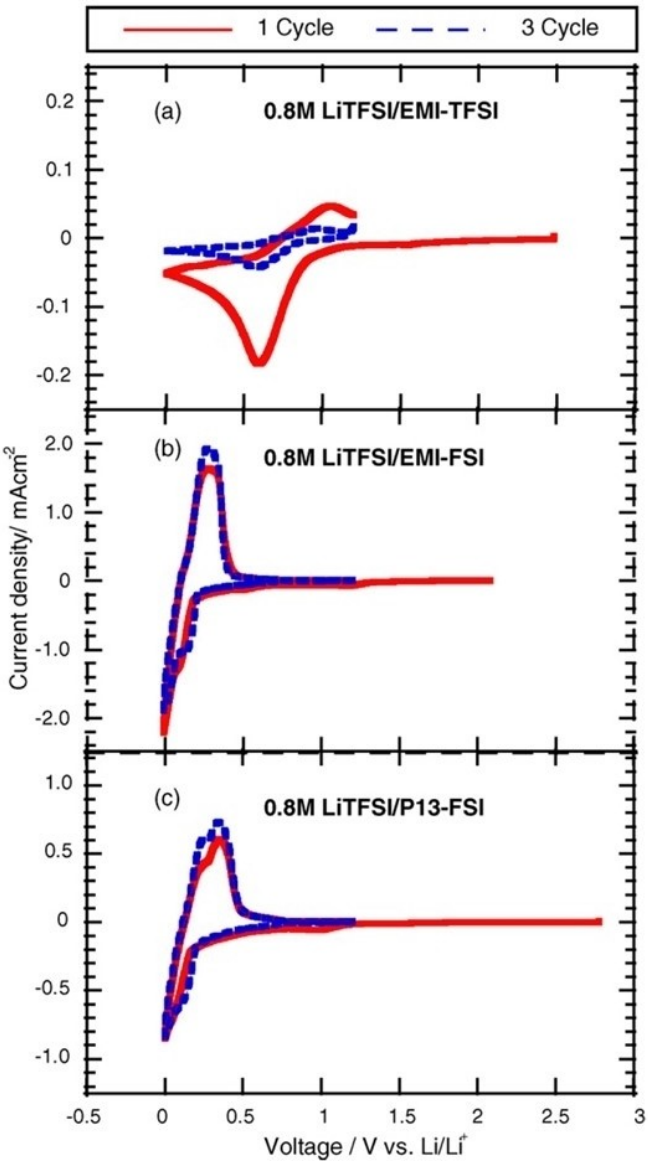

Figure 5. Cyclic voltammograms of natural graphite in various ILs. (a) 0.8 M Li[TFSA]–[C_2C_1im][TFSA], (b) 0.8 M Li[TFSA]–[C_2C_1im][FSA], and (c) 0.8 M Li[TFSA]–[C_3C_1pyrr][FSA]. Reproduced from Ref. [15f] with permission from Elsevier.

[FSA]–[C_3C_1pyrr][FSA] was increased from 0.20 to 0.40.[36a] We further investigated the performance of HC/$NaCrO_2$ full-cells with a Na metal reference electrode and evaluated the charge–discharge behaviors of positive and negative electrodes separately.[36d] As the charge–discharge rate increased, larger potential polarizations were observed at the positive and negative electrodes during discharging and charging, respectively. This indicates the depletion of Na^+ ions in the IL electrolytes inside the composite electrodes, where the Na^+ ion insertion reaction occurs (Figure 8). Therefore, the full-cell

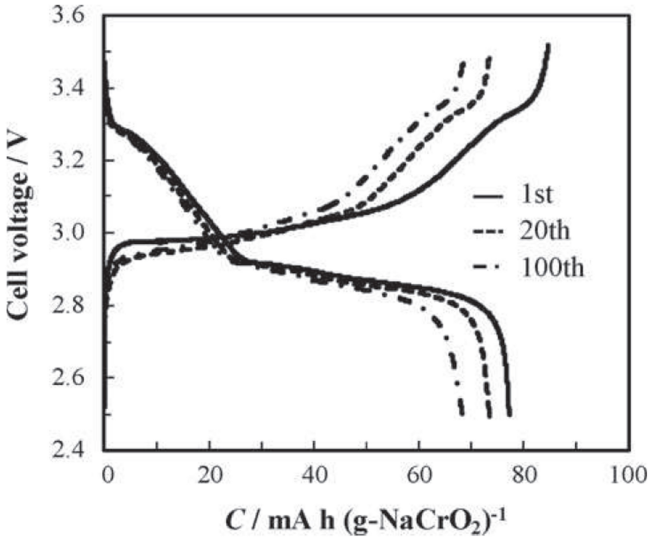

Figure 6. Charge–discharge curves for a Na/$NaCrO_2$ cell using the Na-[FSA]–K[FSA] (x(Na[FSA]) = 0.56) electrolyte at 353 K. Charge–discharge rate: 15 mA g^{-1}. Reproduced from Ref. [32] with permission from Elsevier.

capacity is possibly determined by the capability of supplying Na^+ ions from the bulk electrolyte to the electrolyte inside the composite electrodes.

3.3. Potassium-Ion Batteries

In 2017, we reported the physicochemical and electrochemical properties of K[FSA]–[C_3C_1pyrr][FSA],[37] which was the first study on IL electrolytes for potassium-ion batteries. Based on Arrhenius plots obtained at various K[FSA] compositions (Figure 9), the viscosity and ionic conductivity of the ILs are fitted using VTF (Vogel–Tammann–Fulcher) equations, which are often used for viscous and glass-forming compounds.[38]

$$\eta(T) = A_\eta T^{1/2} \exp\left(\frac{B_\eta}{T - T_{0\eta}}\right) \quad (1)$$

$$\sigma(T) = \frac{A_\sigma}{T^{1/2}} \exp\left(-\frac{B_\sigma}{T - T_{0\sigma}}\right) \quad (2)$$

Here, T is the absolute temperature, $T_{0\eta}$ (or $T_{0\sigma}$) is the ideal glass transition temperature, and A_η (or A_σ) and B_η (or B_σ) are constants related to the frequency factor and activation energy, respectively. Table 2 presents a comparison between the selected properties of different M[FSA]–[C_3C_1pyrr][FSA] (x(M[FSA]) = 0.20; M = Li, Na, and K) ILs at 298 K. The potassium-based IL exhibited an ionic conductivity of 4.8 mS cm^{-1} at 298 K, which was superior to that of its sodium counterpart and comparable to that of its lithium counterpart.

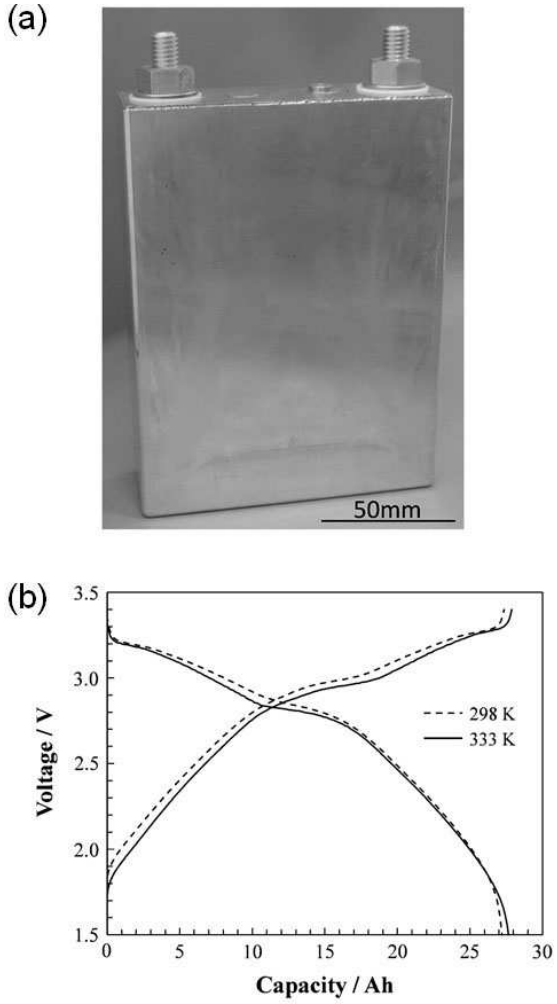

Figure 7. (a) Appearance of a 27 Ah HC/$NaCrO_2$ prismatic full-cell using the Na[FSA]–[C_3C_1pyrr][FSA] (x(Na[FSA]) = 0.20) electrolyte (external size: 113 × 150 × 38 mm; weight: 1.08 kg), and (b) its charge–discharge curves at 298 and 333 K. Charge–discharge rate: 2.7 A (298 K) and 10 A (333 K). Reproduced from Ref. [35h] with permission from Springer.

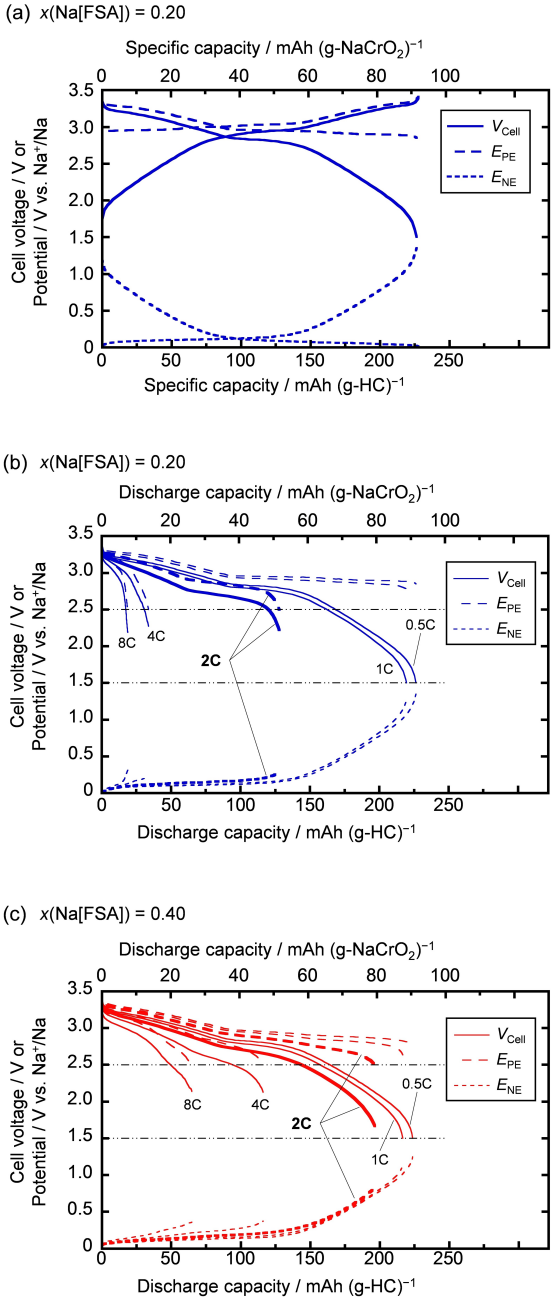

Figure 8. (a) Charge–discharge curves of a HC/$NaCrO_2$ full-cell using the Na[FSA]–[C_3C_1pyrr][FSA] (x(Na[FSA]) = 0.20) electrolyte at 333 K. Charge–discharge rate: 0.5 C (1 C = 100 mA (g-$NaCrO_2$)$^{-1}$). Legends, V_{Cell}, E_{PE}, and E_{NE} are the cell voltage, potential of the $NaCrO_2$ positive electrode, and potential of the HC negative electrode, respectively. (b and c) Discharge curves of the HC/$NaCrO_2$ full-cells using the Na[FSA]–[C_3C_1pyrr][FSA] electrolyte (x(Na[FSA]) = (b) 0.20 and (c) 0.40) at 333 K. Charge rate: 0.5 C. Discharge rates: 0.5–8 C. Reproduced from Ref. [36d] with permission from The Electrochemical Society of Japan.

Figure 10 shows the electrochemical windows of M-[FSA]–[C_3C_1pyrr][FSA] (x(M[FSA]) = 0.20; M = Li, Na, and K) ILs at 298 K. The redox potential of K^+/K is more negative than that of Na^+/Na by 0.35 V and that of Li^+/Li by 0.24 V. The potential difference between the Li^+/Li and K^+/K redox couples is larger than that of typical organic solvents,[37] which indicates that potassium-ion batteries with operating voltages higher than that of lithium-ion batteries can be constructed using this IL electrolyte. Similar trends were observed for M[FSA]–[C_2C_1im][FSA] (x(M[FSA]) = 0.20; M = Li, Na, and K) ILs.[39] Our group applied the K[FSA]–[C_3C_1pyrr][FSA] electrolytes to potassium-ion batteries and confirmed good charge–discharge performances for tin-based alloys[40] and graphite[41] negative electrodes as well as graphite/K_2Mn[Fe(CN)$_6$] full cells.[42] After we reported the K-[FSA]–[C_3C_1pyrr][FSA] system, it has been widely used by

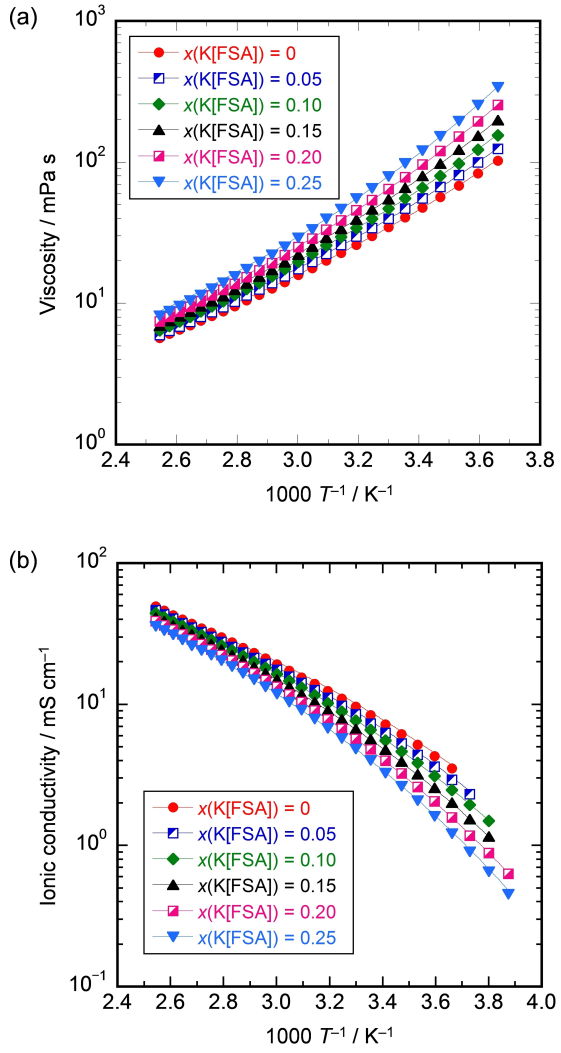

Figure 9. Arrhenius plots of (a) viscosities and (b) ionic conductivities for K[FSA]–[C_3C_1pyrr][FSA] (x(K[FSA]) = 0, 0.05, 0.10, 0.15, 0.20, and 0.25) ILs. Reproduced from Ref. [37] with permission from American Chemical Society.

other groups owing to its high compatibility with various electrodes.[43] We also conducted a comparative study on graphite negative electrodes in M[FSA]–[C_3C_1pyrr][FSA] (x-(M[FSA]) = 0.20; M = Li, Na, and K) electrolytes.[41] We revealed that the formation potentials of binary alkali-metal graphite intercalation compounds (GICs) were localized below −2.85 V vs. Fc^+/Fc (Fc = ferrocene), which was assigned as the virtual onset potential of GIC formation, as shown in Figure 11. Consequently, the difficulty of binary Na-GIC formation with low stage indices can be explained by the small margin between the onset potential and Na^+/Na potential (−2.96 V vs. Fc^+/Fc). In essence, the occurrence of Na metal deposition dominates over Na^+ ion intercalation into graphite. Recently, Kaushik et al. reported that an inorganic IL K[FSA]–Cs[FSA] (x(K[FSA]) = 0.54) was successfully applied as the electrolyte in potassium-ion batteries in combination with graphite negative electrodes at 343 K.[44] The absence of organic cations facilitated stability at elevated temperatures; however, the melting point of this IL was as high as 336 K.[12b]

4. FTA-Based ILs and Other Asymmetric Amide Anions

As mentioned in the introduction, asymmetric anions can effectively decrease the melting points of ILs by preventing close packing between the cations and anions.[13b] The lower melting points of ILs compared to those of traditional molten salts can be explained clearly using recent results obtained through quantum chemical calculations and molecular dynamics simulations. Endo et al. revealed that structural entropies, particularly configurational (intermolecular) entropies, dominantly contribute to the large entropies of ILs.[45] A similar interpretation can be applied to explain the lower melting points of ILs with asymmetric anions.

4.1. Lithium-Based Batteries

In the 2000s, ILs with several asymmetric anions, such as FTA^-, $N(SO_2CF_3)(COCF_3)^-$ ($TSAC^-$, 2,2,2-trifluoro-*N*-(trifluoromethylsulfonyl)acetamide), $N(SO_2C_2F_5)(SO_2CF_3)^-$ ($PTFSA^-$ or $C_1C_2^-$, (pentafluoroethylsulfonyl)(trifluoromethylsulfonyl)amide), were applied as the electrolytes for lithium-ion batteries.[13b,15c] Although TSAC-based ILs showed lower viscosities and higher ionic conductivities than TFSA-based ILs, their reductive stability was low, which reflected in the performance of Li/$LiCoO_2$ cells.[15c] $PTFSA^-$ anion possesses electrochemical stability comparable to $TFSA^-$; however,

Table 2. Physicochemical and electrochemical properties of M[FSA]–[C_3C_1pyrr][FSA] (M = Li, Na, and K) ILs at 298 K.

M	σ / mS cm^{-1}	η / mPa s	ρ / g cm^{-3}	Limit potential vs. Fc^+/Fc / V [37]		E.W. / V [37]
				Cathode	Anode	
Li	5.0 [56]	71.0 [56]	1.4022 [56]	−3.31	2.41	5.48
Na	3.6 [35e]	95 [35e]	1.4127 [35e]	−2.96	2.46	5.42
K	4.8 [37]	78.2 [37]	1.4198 [37]	−3.07	2.41	5.72

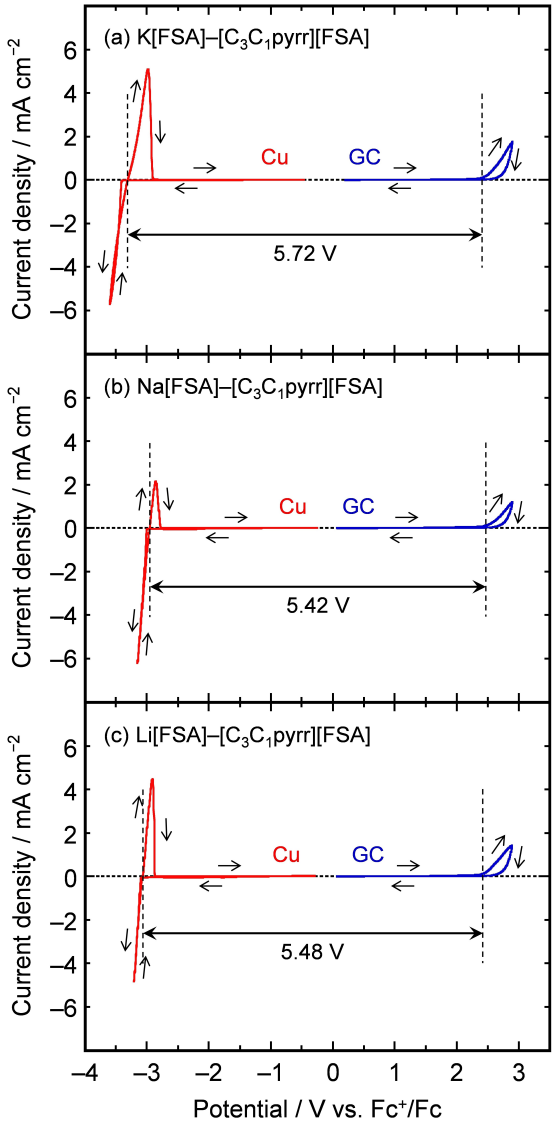

Figure 10. Cyclic voltammograms of copper disk (cathode limit) and glassy carbon disk (anodic limit) in (a) K[FSA]–[C_3C_1pyrr][FSA] (x(K[FSA]) = 0.20), (b) Na[FSA]–[C_3C_1pyrr][FSA] (x(Na[FSA]) = 0.20), and (c) Li-[FSA]–[C_3C_1pyrr][FSA] (x(Li[FSA]) = 0.20) electrolytes at 298 K. Scan rate: 5 mV s^{-1}. Cycle number: 1st. Cathode and anode limits of each electrolyte are indicated by dashed lines. Reproduced from Ref. [37] with permission from American Chemical Society.

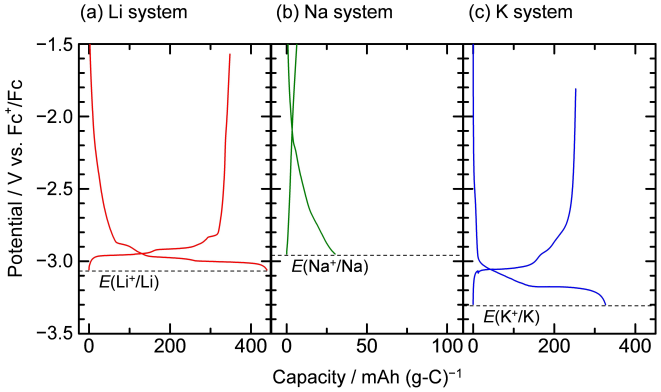

Figure 11. Initial charge–discharge curves of M/graphite half-cells (M = Li, Na, and K) using the M[FSA]–[C_3C_1pyrr][FSA] (x(M[FSA]) = 0.20, M = Li, Na, and K) electrolyte at 298 K. Corresponding alkali metals were used as reference electrodes in a three-electrode cell configuration. Current densities: 37.2, 1.5, and 27.9 mA g^{-1} for Li-, Na-, and K-ion systems, respectively. Reproduced from Ref. [41] with permission from Electrochemical Society.

PTFSA-based ILs are more viscous owing to their bulkiness.[15c] ILs based on another asymmetric anion, $N(SO_2F)(SO_2C_2F_5)^-$ ($FPFSA^-$, (fluorosulfonyl)(pentafluoroethanesulfonyl)amide), were explored.[46] The FPFSA-based ILs showed ionic conductivities and electrochemical stabilities comparable to those of TFSA-based ILs, and also possessed lower melting points. In 2008, Matsumoto et al. reported the physicochemical properties of various ILs with FTA^- anions, which exhibited significantly lower melting points than ILs with other amide anions.[13c] Subsequently, various FTA-based ILs with Li^+ and organic cations were developed and applied to both lithium-ion batteries[13e,47] and dual-carbon batteries.[48]

Similar to FSA systems, M[FTA] ILs without organic cations appear as electrolytes with low melting points for this kind of ILs.[13d,49] Li[FTA] single salt melts at 373 K and can be used as a single cation ionic liquid (SCIL) electrolyte in Li/$LiCoO_2$ and Li/$LiFePO_4$ batteries at 383 K.[49a] Since SCILs contain single alkali metal cations without any neutral solvents or organic ILs, they cannot be diluted. Thus, they are intrinsically unrelated to the decrease in concentration of alkali metal cations on the electrode surface. In addition, SCILs generally have a high cation transference number, which is advantageous over organic solvent-based electrolytes and organic ILs of the same conductivity. Furthermore, a Li-[FTA]–Cs[FTA] (x(Li[FTA]) = 0.40) binary IL was applied as the electrolyte of lithium-ion batteries operating at 318–383 K, in which $LiCoO_2$ and $LiFePO_4$ positive electrodes and a graphite negative electrode functioned successfully (Figure 12).[49b,c]

4.2. Other Rechargeable Batteries

In 2020, Yang et al. conducted systematic studies on a Na[FTA]–[C_4C_1pyrr][FTA] system as the electrolyte of sodium-ion batteries, and investigated the effects of the Na^+ ion concentration on the electrochemical behavior of Na/Na symmetric cells and Na/HC half-cells.[23b] We reported the physicochemical and electrochemical properties of M-[FTA]–[C_4C_1pyrr][FTA] ILs (x(M[FTA]) = 0.20; M = Li, Na, K, Rb, and Cs) as the electrolytes of alkali metal-ion batteries and revealed that the trend of ionic conductivities of these ILs

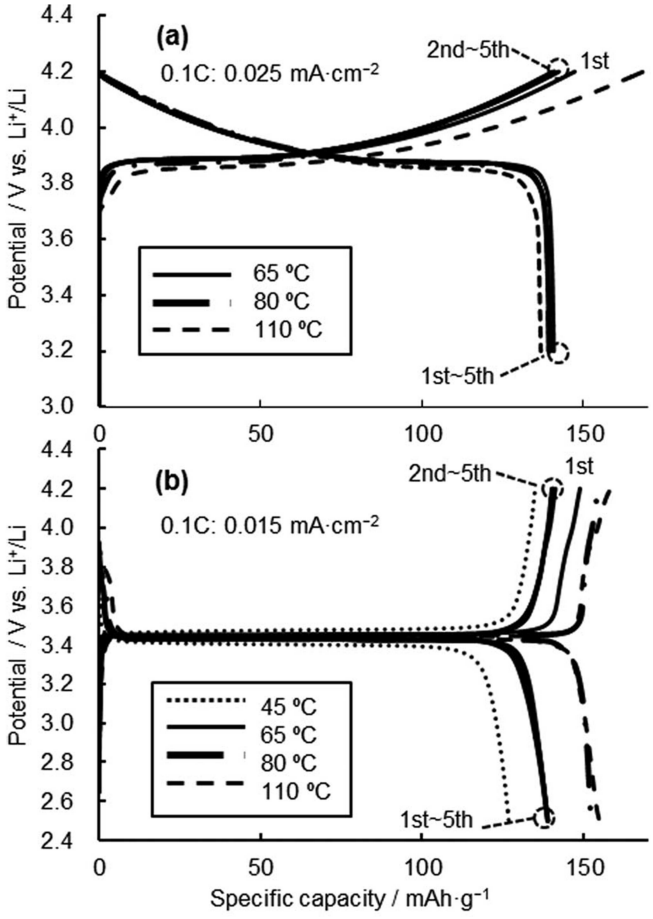

Figure 12. Charge–discharge curves of (a) Li/$LiCoO_2$ cell and (b) Li/$LiFePO_4$ cell using the Li[FTA]–Cs[FTA] (x(Li[FTA]) = 0.40) electrolyte at 45–110 °C. Charge–discharge rate: 0.1 C ($LiCoO_2$: 0.025 mA cm^{-2}; $LiFePO_4$: 0.015 mA cm^{-2}). Reproduced from Ref. [49b] with permission from Electrochemical Society.

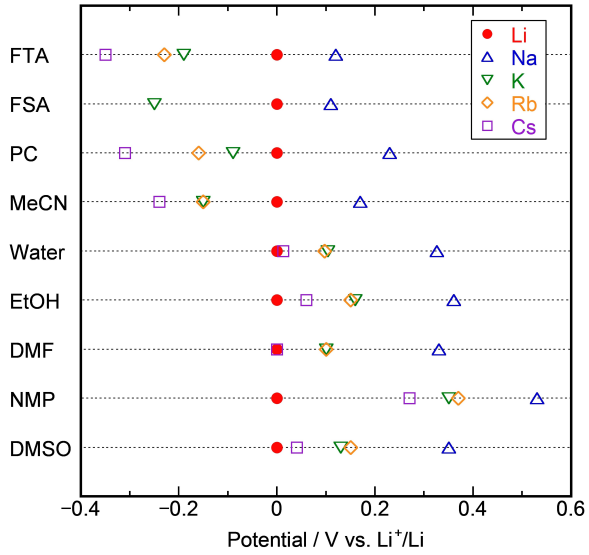

Figure 13. Redox potentials of alkali metals (E(M^+/M); M = alkali metal) in various electrolytes with respect to E(Li^+/Li). FTA = M-[FTA]–[C_4C_1pyrr][FTA] (C(Li^+) = 0.820 mol dm^{-3}, C(Na^+) = 0.819 mol dm^{-3}, C(K^+) = 0.814 mol dm^{-3}, C(Rb^+) = 0.811 mol dm^{-3}, and C(Cs^+) = 0.806 mol dm^{-3}), FSA = M[FSA]–[C_3C_1pyrr][FSA] (C(Li^+) = 0.99 mol dm^{-3}, C(Na^+) = 0.98 mol dm^{-3},[35e] and C(K^+) = 0.98 mol dm^{-3}),[37] PC = propylene carbonate (C(M^+) = 1 mol dm^{-3}), MeCN = acetonitrile (C(M^+) = 1 mol dm^{-3}), EtOH = ethanol (C(M^+) = 1 mol dm^{-3}), DMF = *N*,*N*-dimethylformamide (C(M^+) = 1 mol dm^{-3}), NMP = *N*-methylpyrrolidone (C(M^+) = 1 mol dm^{-3}), and DMSO = dimethyl sulfoxide (C(M^+) = 1 mol dm^{-3}). Reproduced from Ref. [50] with permission from American Chemical Society.

at 298 K could be explained by the charge densities of alkali metal cations, except for the Li-based system.[50] Moreover, the values of the M^+/M redox potential increased as follows: Cs < Rb < K < Li < Na, which indicated that the Cs system exhibited the widest electrochemical window. As shown in Figure 13, the trend of the M^+/M redox potential is similar to that of other ILs and several organic solvents, such as propylene carbonate and acetonitrile, but is different from that of other organic solvents and aqueous solutions.[51] These potential differences should be originated from the coordination environments, i.e., the interactions between alkali metal cations and solvents (or anions). Some trends have been explained by thermodynamic calculations for aqueous solutions and organic solvents.[51] Since ILs are composed entirely of cations and anions and are dominated by ion–ion interactions, it is natural to consider that smaller cations induce stronger ion–ion interactions which may lead to high electrochemical stability (more negative redox potential of alkali metals). However, the obtained results cannot be simply explained by this hypothesis, indicating that other factors should affect the unexplained trends in ILs. We also investigated rubidium intercalation/deintercalation into/from graphite in a Rb[FTA]–[C_4C_1pyrr][FTA] IL electrolyte at 298 K, which firstly realized the electrochemical formation of a RbC_8 phase at room temperature.[52]

Significantly, SCILs as electrolytes for potassium-ion batteries have been studied by several groups (Figure 14).[53] A K[FSA]–K[FTA] mixture with a composition of x(K[FSA]) = 0.55 was reported to melt at 340 K, and the operation of a graphite negative electrode at 353 K was demonstrated, entailing the formation of a KC_8 phase in the fully charged state.[53a] A room-temperature SCIL was recently realized by mixing K[FSA] and K[MPSA] (MPSA = (3-methoxypropyl)(trifluoromethylsulfonyl)amide) in the compositional range of x(K[FSA]) = 0.50–0.80, which showed an ionic conductivity of approximately 1 mS cm^{-1} at x(K[FSA]) = 0.50 at 328 K.[53b]

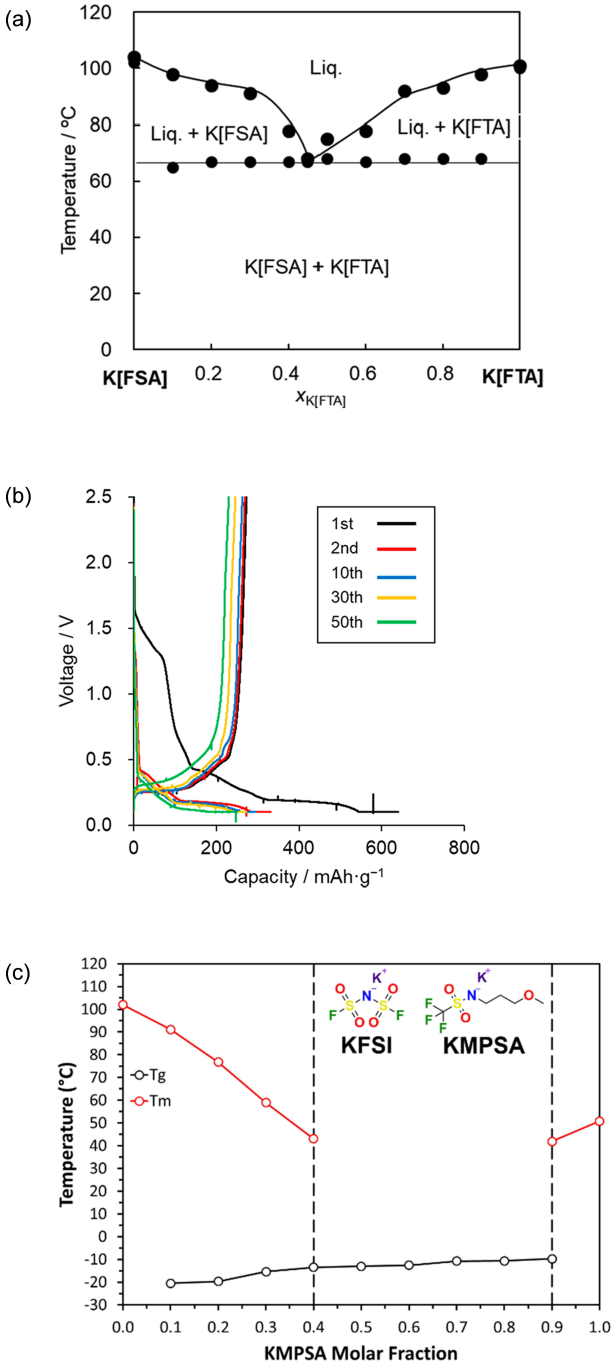

Figure 14. (a) Phase diagram of the K[FSA]−K[FTA] binary system determined through differential scanning calorimetry (DSC), and (b) charge−discharge curves of a K/graphite cell using the $K[FSA]_{0.55}[FTA]_{0.45}$ SCIL at 80°C and a charge–discharge rate of 0.3 C. Reproduced from Ref. [53a] with permission from American Chemical Society. (c) Phase diagram of the K[FSA]–K[MPSA] binary system determined through DSC analysis (T_m: melting point; T_g: glass transition temperature). Reproduced from Ref. [53b] with permission from American Chemical Society.

5. Summary and Outlook

Herein, we have introduced the history and contributions to the development of alkali metal-ion batteries that utilize IL electrolytes. In general, FSA-ILs are promising electrolytes because they exhibit low melting points, high ionic conductivities, and low interfacial resistance by forming highly compatible SEI formation. We have also focused on the application of FSA-ILs, particularly in sodium- and potassium-ion batteries. Although the electrolyte properties of FSA-ILs are favorable as described above, they are still somewhat inferior to those of conventional organic-solvent-based electrolytes in some respects. A distinctive feature of ILs is that they are composed entirely of ions, that is, all components of ILs can be charge carriers. In particular, the ILs with high M^+ concentrations are known to deliver high electrochemical performance in rechargeable batteries. Since the mechanism has not yet been elucidated, this research field is of great interest for the future. In the same context, SCILs, which can be regarded as an ultimate high concentration IL, are also an interesting research topic, although they works at elevated temperatures over 343 K. Moreover, ionic plastic crystals, one of the IL derivatives, could be promising candidates because they exhibit high ionic conductivities as solid electrolytes in the temperature range below the melting point. Finally, ILs potentially enable us to construct rechargeable batteries with high performance and high safety towards the practical applications. We hope that this research field will further prosper in the future.

Acknowledgements

This study was partly supported by the Advanced Low Carbon Technology Research and Development Program (ALCA) of the Japan Science and Technology Agency (JST), the MEXT program "Elements Strategy Initiative to Form Core Research Center" (MEXT: Ministry of Education Culture, Sports, Science, and Technology, Japan), and JSPS KAKENHI grants (JP18 K14320 and JP21 K14718).

Data Availability Statement

Data sharing is not applicable to this article as no new data were created or analyzed in this study.

References

[1] a) R. Hagiwara, K. Matsumoto, J. Hwang, T. Nohira, *Chem. Rec.* **2019**, *19*, 758–770; b) T. Yamamoto, *Electrochemistry* **2022**, *90*, 101005.

[2] a) M. Watanabe, M. L. Thomas, S. Zhang, K. Ueno, T. Yasuda, K. Dokko, *Chem. Rev.* **2017**, *117*, 7190–7239; b) H. Nakamoto, M. Watanabe, *Chem. Commun.* **2007**, 2539–2541; c) J. S. Lee, T. Nohira, R. Hagiwara, *J. Power Sources* **2007**, *171*, 535–539; d) M. Ue, M. Takeda, A. Toriumi, A. Kominato, R. Hagiwara, Y. Ito, *J. Electrochem. Soc.* **2003**, *150*, A499–A502.

[3] a) R. R. Deshmukh, R. Rajagopal, K. V. Srinivasan, *Chem. Commun.* **2001**, 1544–1545; b) N. Koura, H. Nagase, A. Sato, S. Kumakura, K. Takeuchi, K. Ui, T. Tsuda, C. K. Loong, *J. Electrochem. Soc.* **2008**, *155*, D155–D157; c) K. Matsumoto, K. Shima, T. Sugimoto, T. Inoue, R. Hagiwara, *Angew. Chem. Int. Ed.* **2021**, *133*, 7966–7971.

[4] a) M. Ramdin, T. W. de Loos, T. J. H. Vlugt, *Ind. Eng. Chem. Res.* **2012**, *51*, 8149–8177; b) H. Takana, N. Hara, T. Makino, M. Kanakubo, *J. Electrost.* **2021**, *114*, 103634.

[5] a) S. Dutta, S. Pal, *Biomass Bioenergy* **2014**, *62*, 182–197; b) K. Ninomiya, A. R. I. Utami, Y. Tsuge, K. Kuroda, C. Ogino, T. Taima, J. Saito, M. Kimizu, K Takahashi, *Chem. Eng. J.* **2018**, *334*, 657–663; c) T. Kodaki, T. Kishiro, Y. Sugie, T. Nohira, *J. Jpn. Inst. Energy* **2022**, *101*, 83–87.

[6] a) H. Satria, K. Kuroda, Y. Tsuge, K. Ninomiya, K. Takahashi, *New J. Chem.* **2018**, *42*, 13225–13228; b) T. Hirata, T. Takekiyo, Y. Yoshimura, Y. Tokoro, T. Ishizaki, Y. Kizuka, K. Kuroda, *RSC Adv.* **2022**, *12*, 11628–11631.

[7] a) D. Brouillette, D. E. Irish, N. J. Taylor, Gérald Perron, M. Odziemkowskic, J. E. Desnoyers, *Phys. Chem. Chem. Phys.* **2002**, *4*, 6063–6071; b) J.-F. Huang, H. Luo, S. Dai, *J. Electrochem. Soc.* **2006**, *153*, J9–J13; c) T. Tamura, T. Hachida, K. Yoshida, N. Tachikawa, K. Dokko, M. Watanabe, *J. Power Sources* **2010**, *195*, 6095–6100; d) C. A. Angell, Y. Ansari, Z. Zhao, *Faraday Discuss.* **2012**, *154*, 9–27.

[8] a) D. R. Vissers, Z. Tomczuk, R. K. Steunenberg, *J. Electrochem. Soc.* **1974**, *121*, 665–667; b) E. C. Gay, D. R. Vissers, F. J. Martino, K. E. Anderson, *J. Electrochem. Soc.* **1976**, *123*, 1591–1596; c) T. Kasajima, T. Nishikiori, T. Nohira, Y. Ito, *Electrochem. Solid-State Lett.* **2003**, *6*, A109–A112.

[9] a) R. T. Carlin, H. C. De Long, J. Fuller, P. C. Trulove, *J. Electrochem. Soc.* **1994**, *141*, L73–L76; b) R. T. Carlin, J. Fuller, W. K. Kuhn, M. J. Lysaght, P. C. Trulove, *J. Appl. Electrochem.* **1996**, *26*, 1147–1160; c) Y. S. Fung, R. Q. Zhou, *J. Power Sources* **1999**, *81–82*, 891–895.

[10] a) J. S. Wilkes, M. J. Zaworotko, *J. Chem. Soc. Chem. Commun.* **1992**, 965–967; b) V. R. Koch, L. A. Dominey, C. Nanlundiah, *J. Electrochem. Soc.* **1996**, *143*, 798–803; c) P. Bonhôte, A.-P. Dias, N. Papageorgiou, K. Kalyanasundaram, M. Grätzel, *Inorg. Chem.* **1996**, *35*, 1168–1178; d) J. Fuller, R. T. Carlin, R. A. Osteryoung, *J. Electrochem. Soc.* **1997**, *144*, 3881–3886.

[11] a) R. Hagiwara, K. Tamaki, K. Kubota, T. Goto, T. Nohira, *J. Chem. Eng. Data* **2008**, *53*, 355–358; b) A. Watarai, K. Kubota, M. Yamagata, T. Goto, T. Nohira, R. Hagiwara, K. Ui, N. Kumagai, *J. Power Sources* **2008**, *183*, 724–729; c) T. Nohira, T. Ishibashi, R. Hagiwara, *J. Power Sources* **2012**, *205*, 506–509.

[12] a) K. Kubota, T. Nohira, T. Goto, R. Hagiwara, *Electrochem. Commun.* **2008**, *10*, 1886–1888; b) K. Kubota, T. Nohira, R. Hagiwara, *J. Chem. Eng. Data* **2010**, *55*, 3142–3146.

[13] a) H. Matsumoto, H. Kageyama, Y. Miyazaki, *Chem. Commun.* **2002**, 1726–1727; b) H. Matsumoto, H. Sakaebe, K. Tatsumi, *J. Power Sources* **2005**, *146*, 45–50; c) H. Matsumoto, N. Terasawa, T. Umecky, S. Tsuzuki, H. Sakaebe, K. Asaka, K. Tatsumi, *Chem. Lett.* **2008**, *37*, 1020–1021; d) K. Kubota, T. Nohira, R. Hagiwara, H. Matsumoto, *Chem. Lett.* **2010**, *39*, 1303–1304; e) J. Reiter, S. Jeremias, E. Paillard, M. Winter, S. Passerini, *Phys. Chem. Chem. Phys.* **2013**, *15*, 2565–2571.

[14] a) D. R. MacFarlane, P. Meakin, J. Sun, N. Amini, M. Forsyth, *J. Phys. Chem. B* **1999**, *103*, 4164–4170; b) H. Matsumoto, M. Yanagida, K. Tanimoto, T. Kojima, Y. Tamiya, Y. Miyazaki, edited by P. C. Trulove et al., *Molten salts XII*, Electrochem. Soc., Pennington, NJ, **2000**, p. 186–192; c) H. Matsumoto, M. Yanagida, K. Tanimoto, M. Nomura, Y. Kitagawa, Y. Miyazaki, *Chem. Lett.* **2000**, *29*, 922–923; d) H. Matsumoto, H. Kageyama, Y. Miyazaki, *Chem. Lett.* **2001**, *30*, 182–183.

[15] a) H. Sakaebe, H. Matsumoto, *Electrochem. Commun.* **2003**, *5*, 594–598; b) B. Garcia, S. Lavallée, G. Perron, C. Michot, M. Armand, *Electrochim. Acta* **2004**, *49*, 4583–4588; c) H. Sakaebe, H. Matsumoto, K. Tatsumi, *J. Power Sources* **2005**, *146*, 693–697; d) H. Sakaebe, H. Matsumoto, K. Tatsumi, *Electrochim. Acta* **2007**, *53*, 1048–1054; e) P. C. Howlett, N. Brack, A. F. Hollenkamp, M. Forsyth, D. R. MacFarlane, *J. Electrochem. Soc.* **2006**, *153*, A595–A606; f) M. Ishikawa, T. Sugimoto, M. Kikuta, E. Ishiko, M. Kono, *J. Power Sources* **2006**, *162*, 658–662.

[16] a) G. H. Newman, L. P. Klemann, *J. Electrochem. Soc.* **1980**, *127*, 2097–2099; b) C. Delmas, J. J. Braconnier, C. Fouassier, P. Hagenmuller, *Solid State Ionics* **1981**, *3–4*, 165–169; c) J. J. Braconnier, C. Delmas, P. Hagenmuller, *Mat. Res. Bull.* **1982**, *17*, 993–1000; d) K. M. Abraham, *Solid State Ionics* **1982**, *7*, 199–212.

[17] a) S. Okada, Y. Takahashi, T. Kiyabu, T. Doi, J. Yamaki, T. Nishida, *210th ECS Meeting Abstracts*, (2006) MA2006-02, 201; b) F. Sauvage, L. Laffont, J.-M. Tarascon, E. Baudrin, *Inorg. Chem.* **2007**, *46*, 3289–3294; c) I. D. Gocheva, M. Nishijima, T. Doi, S. Okada, J. Yamaki, T. Nishida, *J. Power Sources* **2009**, *187*, 247–252; d) L. S. Plashnitsa, E. Kobayashi, Y. Noguchi, S. Okada, J. Yamaki, *J. Electrochem. Soc.* **2010**, *157*, A536–A543; e) S. Komaba, C. Takei, T. Nakayama, A. Ogata, N. Yabuuchi, *Electrochem. Commun.* **2010**, *12*, 355–358.

[18] a) S. R. Taylor, S. M. McLennan, *"The Continental Crust: its Composition and Evolution"*, Blackwell, Oxford, (1985); b) M. S. Quinby-Hunt, K. K. Turehian, *Eos* **1983**, *64*, 130–132.

[19] D. Monti, E. Jónsson, M. R. Palacín, P. Johansson, *J. Power Sources* **2014**, *245*, 630–636.

[20] a) S. A. M. Noor, P. C. Howlett, D. R. MacFarlane, M. Forsyth, *Electrochim. Acta* **2013**, *114*, 766–771; b) N. Wongittharom, T.-C. Lee, C.-H. Wang, Y.-C. Wang, J.-K. Chang, *J. Mater. Chem. A* **2014**, *2*, 5655–5661.

[21] a) P. Geand, M. Fouletier, *Solid State Ionics* **1988**, *28–30*, 1172–1175; b) M. M. Doeff, Y. Ma, S. J. Visco, L. C. De Jonghe, *J. Electrochem. Soc.* **1993**, *140*, L169–L170.

[22] a) D. A. Stevens, J. R. Dahn, *J. Electrochem. Soc.* **2000**, *147*, 1271–1273; b) D. A. Stevens, J. R. Dahn, *J. Electrochem. Soc.*

2001, *148*, A803–A811; c) S. Komaba, W. Murata, T. Ishikawa, N. Yabuuchi, T. Ozeki, T. Nakayama, A. Ogata, K. Gotoh, K. Fujiwara, *Adv. Funct. Mater.* **2011**, *21*, 3859–3867.

[23] a) M. Egashira, T. Tanaka, N. Yoshimoto, M. Morita, *Electrochemistry* **2012**, *80*, 755–758; b) H. Yang, X.-F. Luo, K. Matsumoto, J.-K. Chang, R. Hagiwara, *J. Power Sources* **2020**, *470*, 228406.

[24] a) A. Eftekhari, *J. Power Sources* **2004**, *126*, 221–228; b) N. Recham, G. Rousse, M. T. Sougrati, J.-N. Chotard, C. Frayret, S. Mariyappan, B. C. Melot, J.-C. Jumas, J.-M. Tarascon, *Chem. Mater.* **2012**, *24*, 4363–4370; c) S. Komaba, T. Hasegawa, M. Dahbi, K. Kubota, *Electrochem. Commun.* **2015**, *60*, 172–175.

[25] a) T. Masese, K. Yoshii, Y. Yamaguchi, T. Okumura, Z.-D. Huang, M. Kato, K. Kubota, J. Furutani, Y. Orikasa, H. Senoh, H. Sakaebe, M. Shikano, *Nat. Commun.* **2018**, *9*, 3823; b) K. Yoshii, T. Masese, M. Kato, K. Kubota, H. Senoh, M. Shikano, *ChemElectroChem* **2019**, *6*, 3901–3910; c) T. Masese, K. Yoshii, K. Tada, M. Kato, S. Uchida, K. Kubota, T. Ina, T. Okumura, Z.-D. Huang, J. Furutani, Y. Orikasa, H. Senoh, S. Tanaka, M. Shikano, *Energy Technol.* **2020**, *8*, 2000039.

[26] a) S. Seki, Y. Kobayashi, H. Miyashiro, Y. Ohno, Y. Mita, N. Terada, P. Charest, A. Guerfi, K. Zaghib, *J. Phys. Chem. C* **2008**, *112*, 16708–16713; b) J. Saint, A. S. Best, A. F. Hollenkamp, J. Kerr, J.-H. Shin, M. M. Doeff, *J. Electrochem. Soc.* **2008**, *155*, A172–A180; c) A. I. Bhatt, A. S. Best, J. Huang, A. F. Hollenkamp, *J. Electrochem. Soc.* **2010**, *157*, A66–A74.

[27] a) H. Matsumoto, H. Sakaebe, K. Tatsumi, M. Kikuta, E. Ishiko, M. Kono, *J. Power Sources* **2006**, *160*, 1308–1313; b) M. Yamagata, N. Nishigakia, S. Nishishita, Y. Matsui, T. Sugimoto, M. Kikuta, T. Higashizaki, M. Kono, M. Ishikawa, *Electrochim. Acta* **2013**, *110*, 181–190.

[28] A. Guerfi, S. Duchesne, Y. Kobayashi, A. Vijh, K. Zaghi, *J. Power Sources* **2008**, *175*, 866–873.

[29] M. Yamagata, K. Tanaka, Y. Tsuruda, Y. Sone, S. Fukuda, S. Nakasuka, M. Kono, M. Ishikawa, *Electrochemistry* **2015**, *83*, 918–924.

[30] a) K. Hayamizu, S. Tsuzuki, S. Seki, Y. Umebayashi, *J. Chem. Phys.* **2011**, *135*, 084505; b) K. Fujii, H. Hamano, H. Doi, X. Song, S. Tsuzuki, K. Hayamizu, S. Seki, Y. Kameda, K. Dokko, M. Watanabe, Y. Umebayashi, *J. Phys. Chem. C* **2013**, *117*, 19314–19324.

[31] a) W. A. Henderson, S. Passerini, *Chem. Mater.* **2004**, *16*, 2881–2885; b) H. Yoon, A. S. Best, M. Forsyth, D. R. MacFarlane, P. C. Howlett, *Phys. Chem. Chem. Phys.* **2015**, *17*, 4656–4663.

[32] A. Fukunaga, T. Nohira, Y. Kozawa, R. Hagiwara, S. Sakai, K. Nitta, S. Inazawa, *J. Power Sources* **2012**, *209*, 52–56.

[33] a) T. Yamamoto, T. Nohira, R. Hagiwara, A. Fukunaga, S. Sakai, K. Nitta, S. Inazawa, *J. Power Sources* **2012**, *217*, 479–484; b) T. Yamamoto, T. Nohira, R. Hagiwara, A. Fukunaga, S. Sakai, K. Nitta, S. Inazawa, *J. Power Sources* **2013**, *237*, 98–103; c) T. Yamamoto, T. Nohira, R. Hagiwara, A. Fukunaga, S. Sakai, K. Nitta, and S. Inazawa, *Electrochim. Acta* **2014**, *135*, 60–67; d) C.-Y. Chen, K. Matsumoto, T. Nohira, R. Hagiwara, A. Fukunaga, S. Sakai, K. Nitta, S. Inazawa, *J. Power Sources* **2013**, *237*, 52–57; e) C.-Y. Chen, K. Matsumoto, T. Nohira, R. Hagiwara, Y. Orikasa, Y. Uchimoto, *J. Power Sources* **2014**, *246*, 783–787.

[34] a) S. A. M. Noor, P. C. Howlett, D. R. MacFarlane, M. Forsyth, *Electrochim. Acta* **2013**, *114*, 766–771; b) D. Monti, E. Jónsson, M. R. Palacín, P. Johansson, *J. Power Sources* **2014**, *245*, 630–636; c) L. G. Chagas, D. Buchholz, L. Wu, B. Vortmann, S. Passerini, *J. Power Sources* **2014**, *247*, 377–383; d) H. Yoon, H. Zhu, A. Hervault, M. Armand, D. R. MacFarlane, M. Forsyth, *Phys. Chem. Chem. Phys.* **2014**, *16*, 12350–12355.

[35] a) C. Ding, T. Nohira, K. Kuroda, R. Hagiwara, A. Fukunaga, S. Sakai, K. Nitta, S. Inazawa, *J. Power Sources* **2013**, *238*, 296–300; b) A. Fukunaga, T. Nohira, R. Hagiwara, K. Numata, E. Itani, S. Sakai, K. Nitta, S. Inazawa, *J. Power Sources* **2014**, *246*, 387–391; c) C.-Y. Chen, K. Matsumoto, T. Nohira, C. Ding, T. Yamamoto, R. Hagiwara, *Electrochim. Acta* **2014**, *133*, 583–588; d) K. Matsumoto, T. Hosokawa, T. Nohira, R. Hagiwara, A. Fukunaga, K. Numata, E. Itani, S. Sakai, K. Nitta, S. Inazawa, *J. Power Sources* **2014**, *265*, 36–39; e) K. Matsumoto, Y. Okamoto, T. Nohira, R. Hagiwara, *J. Phys. Chem. C* **2015**, *119*, 7648–7655; f) K. Matsumoto, R. Taniki, T. Nohira, R. Hagiwara, *J. Electrochem. Soc.* **2015**, *162*, A1409–A1414; g) T. Hosokawa, K. Matsumoto, T. Nohira, R. Hagiwara, A. Fukunaga, S. Sakai, K. Nitta, *J. Phys. Chem. C* **2016**, *120*, 9628–9636; h) A. Fukunaga, T. Nohira, R. Hagiwara, K. Numata, E. Itani, S. Sakai, K. Nitta, *J. Appl. Electrochem.* **2016**, *46*, 487–496.

[36] a) C. Ding, T. Nohira, R. Hagiwara, K. Matsumoto, Y. Okamoto, A. Fukunaga, S. Sakai, K. Nitta, S. Inazawa, *J. Power Sources* **2014**, *269*, 124–128; b) C.-Y. Chen, T. Kiko, T. Hosokawa, K. Matsumoto, T. Nohira, R. Hagiwara, *J. Power Sources* **2016**, *332*, 51–59; c) M. Forsyth, H. Yoon, F. Chen, H. Zhu, D. R. MacFarlane, M. Armand, P. C. Howlett, *J. Phys. Chem. C* **2016**, *120*, 4276–4286; d) T. Yamamoto, K. Mitsuhashi, K. Matsumoto, R. Hagiwara, A. Fukunaga, S. Sakai, K. Nitta, T. Nohira, *Electrochemistry* **2019**, *87*, 175–181.

[37] T. Yamamoto, K. Matsumoto, R. Hagiwara, T. Nohira, *J. Phys. Chem. C* **2017**, *121*, 18450–18458.

[38] A. J. Easteal, C. A. Angell, *J. Chem. Phys.* **1972**, *56*, 4231–4233.

[39] T. Yamamoto, R. Matsubara, T. Nohira, *J. Chem. Eng. Data* **2021**, *66*, 1081–1088.

[40] a) Y. Domi, H. Usui, E. Nakabayashi, T. Yamamoto, T. Nohira, H. Sakaguchi, *Electrochemistry* **2019**, *87*, 333–335; b) T. Yamamoto, T. Nohira, *Chem. Commun.* **2020**, *56*, 2538–2541.

[41] T. Yamamoto, A. Yadav, T. Nohira, *J. Electrochem. Soc.* **2022**, *169*, 050507.

[42] H. Onuma, K. Kubota, S. Muratsubaki, T. Hosaka, R. Tatara, T. Yamamoto, K. Matsumoto, T. Nohira, R. Hagiwara, H. Oji, S. Yasuno, S. Komaba, *ACS Energy Lett.* **2020**, *5*, 2849–2857.

[43] a) M. Fiore, S. Wheeler, K. Hurlbutt, I. Capone, J. Fawdon, R. Ruffo, M. Pasta, *Chem. Mater.* **2020**, *32*, 7653–7661; b) M. Kato, T. Masese, K. Yoshii, *New J. Chem.* **2021**, *45*, 4921–4924.

[44] S. Kaushik, K. Kubota, J. Hwang, K. Matsumoto, R. Hagiwara, *ACS Appl. Mater. Interfaces* **2022**, *14*, 14302–14312.
[45] T. Endo, K. Sunada, H. Sumida, Y. Kimura, *Chem. Sci.* **2022**, *13*, 7560–7565.
[46] a) H.-Bo Han, Y.-X. Zhou, K. Liu, J. Nie, X.-J. Huang, M. Armand, Z.-B. Zhou, *Chem. Lett.* **2010**, *39*, 472–474; b) K. Liu, Y.-X. Zhou, H.-B. Han, S.-S. Zhou, W.-F. Feng, J. Nie, H. Li, X.-J. Huang, M. Armand, Z.-B. Zhou, *Electrochim. Acta* **2010**, *55*, 7145–7151.
[47] a) A. Moretti, S. Jeong, G. A. Giffin, S. Jeremias, S. Passerini, *J. Power Sources* **2014**, *269*, 645–650; b) S. Jeong, S. Li, G. B. Appetecchi, Stefano Passerini, *Energy Storage Mater.* **2019**, *18*, 1–9.
[48] a) P. Meister, V. Siozios, J. Reiter, S. Klamor, S. Rothermel, O. Fromm, H.-W. Meyer, M. Winter, T. Placke, *Electrochim. Acta* **2014**, *130*, 625–633; b) K. Beltrop, P. Meister, S. Klein, A. Heckmann, M. Grünebaum, H.-D. Wiemhöfer, M. Winter, T. Placke, *Electrochim. Acta* **2016**, *209*, 44–55.
[49] a) K. Kubota, H. Matsumoto, *J. Phys. Chem. C* **2013**, *117*, 18829–18836; b) K. Kubota, H. Matsumoto, *J. Electrochem. Soc.* **2014**, *161*, A902–A907; c) K. Kubota, H. Matsumoto, *ECS Trans.* **2016**, *73*, 95–100.
[50] T. Yamamoto, S. Nishijima, T. Nohira, *J. Phys. Chem. B* **2020**, *124*, 8380–8387.
[51] Y. Marcus, *Pure Appl. Chem.* **1985**, *57*, 1129–1132.
[52] A. Yadav, H. Kobayashi, T. Yamamoto, T. Nohira, *Electrochemistry* **2023**, *91*, 017002.
[53] a) H. Yamamoto, C.-Y. Chen, K. Kubota, K. Matsumoto, R. Hagiwara, *J. Phys. Chem. B* **2020**, *124*, 6341–6347; b) L. Schkeryantz, P. Nguyen, W. D. McCulloch, C. E. Moore, K. C. Lau, Y. Wu, *J. Phys. Chem. C* **2022**, *126*, 11407–11413.
[54] a) K. Tsunashima, M. Sugiya, *Electrochem. Commun.* **2007**, *9*, 2353–2358; b) K. Tsunashima, A. Kawabata, M. Matsumiya, S. Kodama, R. Enomoto, M. Sugiya, Y. Kunugi, *Electrochem. Commun.* **2011**, *13*, 178–181; c) H.-B. Han, J. Nie, K. Liu, W.-K. Li, W.-F. Feng, M. Armand, H. Matsumoto, Z.-B. Zhou, *Electrochim. Acta* **2010**, *55*, 1221–1226.
[55] K. Matsumoto, E. Nishiwaki, T. Hosokawa, S. Tawa, T. Nohira, R. Hagiwara, *J. Phys. Chem. C* **2017**, *121*, 9209–9219.
[56] T. Nikaido, A. Yadav, T. Yamamoto, T. Nohira, *J. Electrochem. Soc.* **2023**, *170*, 020526.

Manuscript received: May 9, 2023
Revised manuscript received: June 11, 2023
Version of record online: June 30, 2023

